Remote Sensing of Environment 233 (2019) 111374

Contents lists available at ScienceDirect

Remote Sensing of Environment

journal homepage: www.elsevier.com/locate/rse

Assessing spatial-temporal dynamics of urban expansion, vegetation greenness and photosynthesis in megacity Shanghai, China during 2000–2016

Qiaoyan Zhong[a], Jun Ma[a,*], Bin Zhao[a], Xinxin Wang[a], Jiamin Zong[a], Xiangming Xiao[b,**]

[a] Ministry of Education Key Laboratory for Biodiversity Science and Ecological Engineering, Coastal Ecosystems Research Station of the Yangtze River Estuary, and Shanghai Institute of EcoChongming (SIEC), Fudan University, Shanghai 200433, China
[b] Department of Microbiology and Plant Biology, Center for Spatial Analysis, University of Oklahoma, Norman, OK 73019, USA

ARTICLE INFO

Keywords:
Impervious surfaces
Urban vegetation
EVI
GPP
Shanghai
Google Earth Engine

ABSTRACT

Vegetation plays an essential role in improving urban environments and enhancing the physical and mental health of residents. However, rapid urbanization has exerted complicated influence on vegetation conditions, which remain poorly understood. To assess the impacts of urbanization on the vegetation structure and function in the urban area, we quantified the changes in impervious surface area (ISA) and assessed the impacts of urbanization on vegetation greenness (enhanced vegetation index (EVI)), and gross primary production (GPP) in megacity Shanghai during 2000–2016. The results show that 38.0% and 28.0% decreasing trends of EVI and GPP occurred in peri-urban and rural areas due to land use and land cover conversion, whereas 2.8% and 4.6% increasing trends of EVI and GPP occurred in the central city during 2000–2016 in Shanghai. In addition, the enhancement of EVI and GPP owing to the indirect impact of urbanization increased as the impervious surface coverage (ISC) gradient rose and peaked when the ISC reached ~0.8, which compensated for vegetation loss by 24.6% and 17.0%, respectively. The compensation was more stable and significant in peri-urban areas than urban and rural areas. This study provides detailed data and insights on the impacts of urbanization on vegetation, which may help stakeholders to make better management plans for urban vegetation.

1. Introduction

More than half of the world's population now live in towns and cities, and by 2030, the number of the world urban population will swell to approximately 8.6 billion (United Nations, 2017). Vegetation in urban areas plays an indispensable role for people living in urban environments. Urban vegetation can generate multiple environmental benefits, for example, reducing air pollution and the effect of urban heat islands, increasing terrestrial carbon storage, and improving energy conservation and storm water runoff quality (Akbari, 2002; Dwyer et al., 1992; Hardin and Jensen, 2007; Mcpherson and Simpson, 2002; Nowak et al., 2006; Roy et al., 2012). Urban vegetation also provides significant psychological and socioeconomic benefits to local urban residents such as stress relief and increasing property value (Donovan and Butry, 2010; Lohr et al., 2004; Nowak et al., 2002).

Numerous studies have documented the conversion of forest and agricultural land into impervious surface (IS, e.g., roads, houses, buildings) over the decades of urbanization, resulting in dramatic expansion of impervious surfaces (Jr and Gibbons, 1996; Wu and Murray, 2003). Many of those studies used remote sensing technologies to quantify land use and cover conversion, for example, the widespread losses of vegetation area (forest, cropland and wetland) (Deng et al., 2015; Dewan and Yamaguchi, 2009; Li et al., 2006; Salvati and Sabbi, 2011) and vegetation greenness (Liu et al., 2015; Yao et al., 2019; Zhu et al., 2016). Some studies used net primary production (NPP) data from process-based models and data-driven models and reported decrease of NPP in urban areas (Chen et al., 2017; Imhoff et al., 2004; Li et al., 2018; Milesi et al., 2003; Xu et al., 2007; Zhou et al., 2015). Most studies used satellite images (e.g., Landsat, MODIS) in a year or selected years to quantify the changes in ISA and vegetation area (Table 1). There is a need to quantify annual changes in urban land cover types, as the resultant dataset would allow us a better link with annual changes in social-economic factors and policy that drive urban expansion.

All of the above-mentioned studies investigated the direct impact of

* Correspondence to: J. Ma, Ministry of Education Key Laboratory for Biodiversity Science and Ecological Engineering, School of Life Sciences, Fudan University, Shanghai 200433, China.
** Correspondence to: X. Xiao, Department of Microbiology and Plant Biology, University of Oklahoma, Norman, OK 73019, USA.
E-mail addresses: ma_jun@fudan.edu.cn (J. Ma), xiangming.xiao@ou.edu (X. Xiao).

https://doi.org/10.1016/j.rse.2019.111374
Received 13 May 2019; Received in revised form 21 July 2019; Accepted 13 August 2019
0034-4257/

Table 1
A summary on remote sensing research on the impacts of urbanization on urban vegetation.

Vegetation variables	Direct impact		Direct + indirect impacts	
	Selected years data	Time series data	Selected years data	Time series data
Vegetation area	Deng et al., 2015; Dewan and Yamaguchi, 2009; Li et al., 2006; Salvati and Sabbi, 2011;			
Greenness		Liu et al., 2015; Yao et al., 2019; Zhu et al., 2016;	Jia et al., 2018; Zhao et al., 2016;	This study
NPP	Chen et al., 2017; Imhoff et al., 2004; Li et al., 2018; Milesi et al., 2003; Xu et al., 2007;	Zhou et al., 2015;	Peng et al., 2016	Guan et al., 2019;
GPP	Nuarsa et al., 2018;	Liu et al., 2018;		This study

urban expansion on vegetation conditions during the urbanization process. However, vegetation types, structure and functions are complex and dynamic in urban areas, driven by many factors, ranging from urban microclimates to human management practices (e.g., irrigation, fertilization). A number of studies have reported that warmer climates due to urban heat island, increased atmospheric carbon dioxide and nitrogen deposition, along with reinforced human management, promoted the growth of urban vegetation (Calfapietra et al., 2015; Lohse et al., 2008; Lovett et al., 2000; McDonnell et al., 1993). Mcpherson (1998) reported that canopy cover, density and the basal area of trees increased along the rural-urban gradient in Sacramento, California, being mainly attributed to more large, old shaded trees, diverse species, and careful maintenance practices in the urban sector compared to the rural sector. Vallet et al. (2010) found that species in urban woodlands had larger leaf areas, preferences for more base- and nutrient-rich soils and shorter life-span than rural woodlands. Zhao et al. (2016) proposed a conceptual framework for quantifying the impacts of urbanization on vegetation greenness and concluded that vegetation greenness enhancement was prevalent in 32 major cities across China. Their study used the enhanced vegetation index (EVI) to track vegetation growth conditions from the perspective of canopy structure (e.g., leaf area index, greenness), and conducted EVI comparisons among cities. To date, most of previous remote sensing studies reported the effects of urbanization on urban vegetation in the context of single vegetation variable over selected years (Table 1). In order to have a thorough ecological evaluation of urban ecosystems, it is necessary to quantify the changes of two or more vegetation variables over multiple years.

In this study, we studied the impacts of urbanization on urban vegetation greenness (related to canopy structure, e.g., EVI) and vegetation productivity (related to canopy function, e.g., GPP). We selected Shanghai as the study area, as it is a megacity that has witnessed rapid urbanization but has simultaneously preserved parts of rural areas, making this city appropriate for assessing the impacts of urbanization on greenness and GPP of vegetation. Using time-series Landsat satellite imagery and modeling approaches, we aimed to investigate 1) the process and patterns of urban expansion (use IS as an indicator) in Shanghai from 2000 to 2016, 2) the spatial-temporal dynamics of impervious surface coverage (ISC), EVI and GPP from 2000 to 2016, and 3) the impact of urbanization on EVI and GPP along the ISC gradient. We also combined our results with previous studies and field observations to discuss what caused differences in the impacts of urbanization on vegetation: 1) between greenness and GPP and 2) along the ISC gradient. This study provides a comprehensive evaluation of vegetation greenness and GPP in response to urbanization, and the results may have significant implications for urban vegetation management.

2. Materials and methods

2.1. Study area

Shanghai (30°40′N to 31°53′N, 120°52′E to 122°12′E) lies on the east coast of China and covers a total area of 6340.5 km^2 in 2016 (Fig. 1). Given its location on the alluvial plain of the Yangtze River delta, the vast majority of the land area is flat, with an average elevation of 4 m. The city has a humid subtropical climate with four distinct seasons. The monthly mean air temperature ranges from 4.4 °C in January to 29.9 °C in July. Annual mean precipitation is approximately 1600 mm, and > 70% of precipitation is concentrated in the wet season from April to September (Shanghai Statistical Bureau, 2017).

Shanghai is divided into 16 county-level districts, and seven of the districts (Huangpu, Xuhui, Changning, Jing'an, Putuo, Hongkou, and Yangpu) are referred to as the central city (or core urban area), while the others (Pudong, Baoshan, Minhang, Jiading, Jinshan, Songjiang, Qingpu, Fengxian and Chongming) represent peri-urban and rural areas that lie further from the urban core.

Since the “reform and opening-up” policy in 1978, Shanghai has gradually developed into the largest and the most prosperous metropolis in China, accompanied by an increasing acceleration of urbanization. The permanent population grew rapidly from 16.1 million in 2000 to 24.2 million in 2016, according to 2017 human demography statistics. To meet the economic development and people's daily needs, the land used for construction expanded from 2267.8 km^2 in 2003 to 3087.3 km^2 in 2016 (Shanghai Statistical Bureau, 2017).

2.2. Data

2.2.1. Landsat imagery and preprocessing

Shanghai is covered by two (118/038 and 118/039) WRS2 path/rows of Landsat images. We collected all available standard Level 1 Terrain-corrected (L1T) products of the Landsat surface reflectance images on the Google Earth Engine (GEE) platform from 2000 to 2016, including 542 Landsat TM images, 879 Landsat ETM+ images and 230 Landsat OLI images. The CFMask was implemented as the primary algorithm to detect and remove clouds, cloud shadows and snow/ice for Landsat TM, ETM+, and OLI/TIRS products (Foga et al., 2017; USGS, 2015; Zhu et al., 2015; Zhu and Woodcock, 2012).

We calculated two greenness-related spectral indices (NDVI and EVI) and two water-related spectral indices (LSWI and mNDWI) for each Landsat image. NDVI (Tucker, 1979) and EVI (Huete et al., 1997, 2002) were widely used to evaluate the canopy structures (e.g., greenness, leaf area index) of vegetation (Huete et al., 2002). LSWI (Gao, 1996; Xiao et al., 2002a,b) and mNDWI (Xu, 2006) are sensitive to surface water information. The annual maximum NDVI ($NDVI_{max}$) and LSWI ($LSWI_{max}$) were calculated for each year, respectively.

$$NDVI = \frac{\rho_{nir} - \rho_{red}}{\rho_{nir} + \rho_{red}} \quad (1)$$

$$EVI = 2.5 \times \frac{\rho_{nir} - \rho_{red}}{\rho_{nir} + 6 \times \rho_{red} - 7.5 \times \rho_{blue} + 1} \quad (2)$$

$$LSWI = \frac{\rho_{nir} - \rho_{swir}}{\rho_{nir} + \rho_{swir}} \quad (3)$$

$$mNDWI = \frac{\rho_{green} - \rho_{swir}}{\rho_{green} + \rho_{swir}} \quad (4)$$

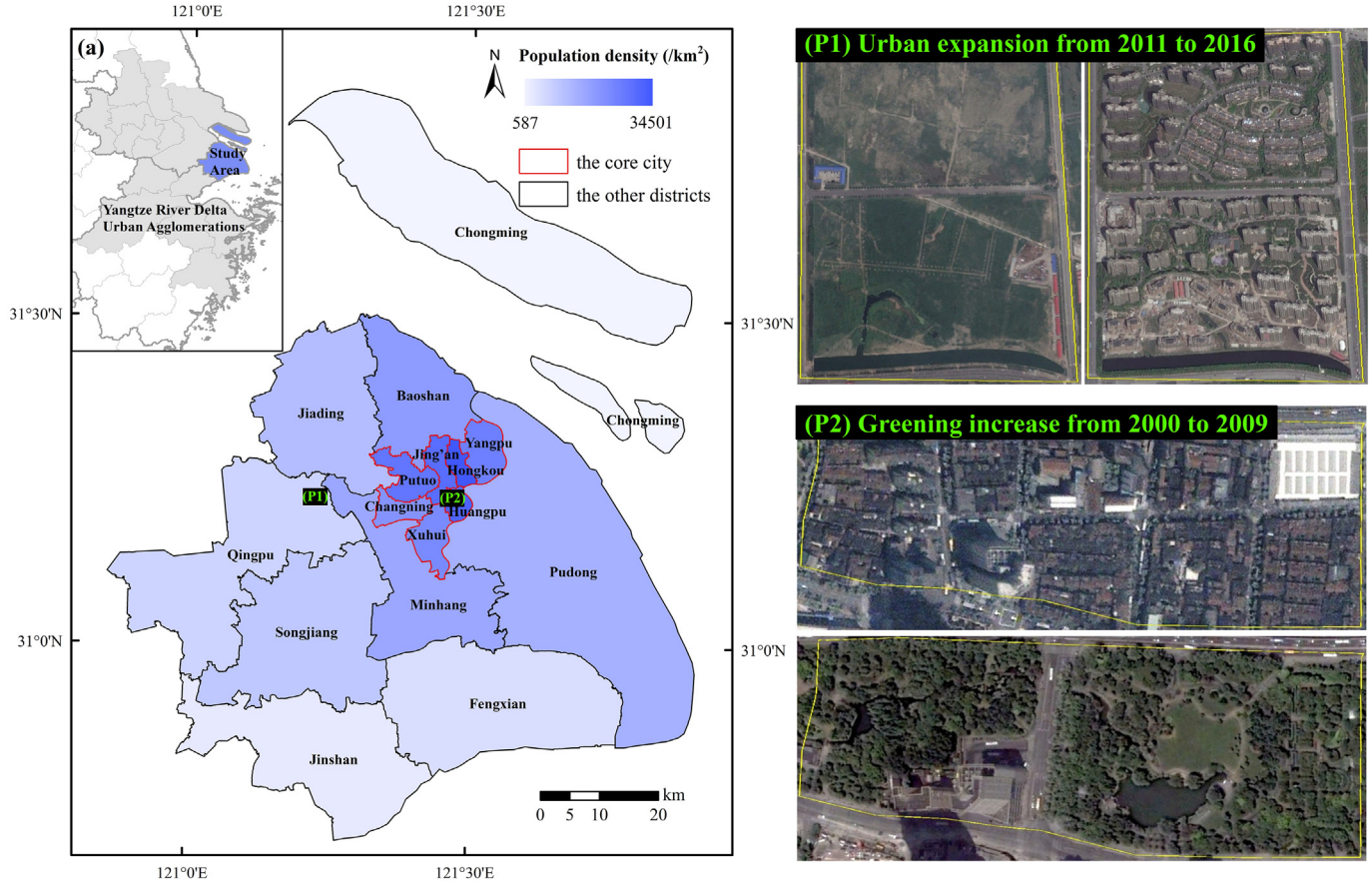

Fig. 1. Population density of individual administrative districts in Shanghai (a). (P1) and (P2) are two examples that use the satellite photos from Google Earth to show the expansion of impervious surface areas (2011–2016) and the increase of greenness (2000–2009) in Shanghai.

where ρ_{blue}, ρ_{green}, ρ_{red}, ρ_{nir}, and ρ_{swir} are Blue (450–520 nm), Green (520–600 nm), Red (B3:630–690 nm), NIR (760–900 nm), and SWIR (1550–1750 nm) bands of the Landsat TM/ETM+/OLI imagery, respectively.

2.2.2. Annual maps of impervious surface during 2000–2016

For simplicity of this study, Landsat images were classified into three broad land cover types: (1) open surface water bodies, (2) impervious surfaces (IS) and (3) other land cover types (e.g., cropland and forest) or "unclassified". We generated annual maps of open surface water bodies, IS and other land cover types (or unclassified) from 2000 to 2016 (17 years, 17 maps).

Open surface water bodies were identified using an algorithm that was documented in previous studies (Zou et al., 2017, 2018). A good-quality observation was identified as an open surface water body if it met the criteria ((mNDWI > NDVI or mNDWI > EVI) and (EVI < 0.1)). We calculated the annual frequency of open surface water bodies for individual pixels in a year, and the pixels with an annual frequency greater than or equal to 0.75 were classified as year-long water bodies (Zou et al., 2017, 2018). We excluded year-long water bodies from the Landsat images for each year to avoid the effect of water bodies on urbanization impact.

Impervious surface is composed of various impenetrable materials with different colors, textures and spectral characteristics. Numerous methods have been successfully applied for identifying and mapping IS using remote sensing approaches at various spatial scales (Kotarba and Aleksandrowicz, 2016; Weng, 2012; Weng et al., 2008; Wu and Murray, 2003; L. Zhang et al., 2017; Y. Zhang et al., 2014). In this study, we used an approach that uses both NDVI and LSWI time series data (Qin et al., 2017), which is based on the fact that IS has low greenness and soil moisture. The annual $NDVI_{max}$ reflects vegetation greenness and leaf area index in a year, whereas the annual $LSWI_{max}$ reflects surface (soil and vegetation) moisture; these were selected to differentiate IS and other land cover types in complex urban-rural areas, including Shanghai (Qin et al., 2017). We performed the spectral analysis of the training data (3000 Region of Interests (ROIs)) and used the threshold values ($NDVI_{max} < 0.6$ and $LSWI_{max} < 0.3$) to identify IS in a year. The criterion of $NDVI_{max} < 0.6$ can exclude most temporary fallow fields and different deciduous forests out of growing season, and the criterion of $LSWI_{max} < 0.3$ can reduce the disturbance of urban waterlogging situation caused by rainy seasons, though it is unusual in Shanghai.

The accuracy of the resultant annual IS maps from Landsat images was assessed using the high-resolution images and photos in Google Earth Pro® (GE) (Luedeling and Buerkert, 2008). The validation data collection strategy was to divide the study area into 5-km by 5-km resolution grid cells (a total of 289 grid cells) and to generate 10 random points within each of the 289 grid cells (a total of 2890 points). We applied the sampling strategy to the land cover maps in 2010 and 2016, and we obtained 2441 points on land and 449 points in the ocean in 2010, as well as 2507 points on land and 383 points in the ocean in 2016. Each point had an acquired buffer zone with 15-m radius (area close to a pixel at 30-m resolution), and only those land points were used for the visual interpretation of very high spatial resolution images and photos. The resultant validation dataset was used to calculate confusion matrices for IS and non-IS.

The resultant annual IS maps with a spatial resolution of 30-m were aggregated spatially into 500-m pixel (matching the pixel size of MODIS images), and the ratios of the IS within 500-m pixels were calculated to support the spatial analysis of EVI and GPP_{VPM} data in Shanghai. We

defined the IS ratio as impervious surface coverage (ISC), which ranged from 0 (full vegetation) to 1 (full IS). Impervious surface area (ISA) and coverage (ISC) in urban areas reflect both the degree of urbanization and the complexity of urban environments (Arnold and Gibbons, 1996; Ridd, 1995).

2.2.3. MODIS land surface reflectance and vegetation index data

The MODIS Terra Surface Reflectance 8-Day product (MOD09A1) provides an estimate of the surface reflectance at 500-m spatial resolution (Vermote, 2015). The clouds, cloud shadows and aerosols were masked based on the quality assurance (QA) layer (Y. Zhang et al., 2016). Considering the low temperature and rainfall in winter (December, January and February), which are unfavorable for vegetation growth, we averaged the EVI of all the available data from March to November for each year during 2000–2016.

2.2.4. The gross primary production (GPP) dataset

The GPP dataset is acquired from the Vegetation Photosynthesis Model (VPM), which is based on light use efficiency theory and is driven by satellite data from MODIS and climate data from NCEP Reanalysis II (Y. Zhang et al., 2017). The GPP_{VPM} dataset includes GPP estimates for all land areas, including urban and rural areas. The GPP_{VPM} data in ten megacities of the world, including Shanghai, were evaluated and compared with the solar-induced chlorophyll fluorescence (SIF) data from the GOME-2 instrument (Cui et al., 2017). Ma et al. (2018) also reported the temporal consistency between GPP_{VPM} and GOME-2 SIF in China during 2010–2014, including urban areas. The raw 500 m 8-day GPP product was temporally aggregated to generate annual GPP from 2000 to 2016.

2.3. Statistical analysis

2.3.1. Spatial-temporal dynamics of ISC, EVI and GPP during 2000–2016

The interannual variation and trends in ISC, EVI and GPP during 2000–2016 at 500-m resolution were calculated and analyzed using linear regression models with *t*-tests at the 5% significance level. The linear relationships between EVI, GPP and ISC were also examined using linear regressions at 500-m resolution in Shanghai from 2000 to 2016.

2.3.2. A conceptual framework for analyzing the impacts of urbanization on EVI and GPP

A conceptual framework was proposed to quantify the impacts of urbanization on vegetation growth, which separated the impacts into direct and indirect impacts (Zhao et al., 2016). The direct impacts induced by land use and cover conversion caused the emergence of the ISC gradient (or urban-rural gradient) in the city during urban expansion. The indirect impacts induced by natural and anthropogenic factors may promote or exacerbate the vegetation conditions during urban development. Theoretically, the vegetation index (VI, i.e., EVI and GPP) of a pixel could be decomposed into contributions from vegetative and nonvegetative areas. Hence, the relationship between VI and ISC should be linear without indirect impacts (Fig. 2a), so the zero-impact straight line was determined by V_v and V_{nv} (Eq. (5)):

$$V_{zi} = (1 - ISC)\cdot V_v + ISC\cdot V_{nv} \quad (5)$$

where V_{zi} was the theoretical VI of a 500-m resolution pixel, V_v was the VI values of a fully vegetated area (ISC = 0, VI = V_v), V_{nv} was the VI values of a fully ISA (ISC = 1, VI = VI_{nv}).

When plotting the VI observations of all pixels against their corresponding ISC along the ISC gradient, the actual distribution of points may not completely be consistent with the straight line, suggesting the existence of indirect impacts (Fig. 2b). The relative indirect impact of urbanization on vegetation growth was calculated as:

$$\omega_i = \frac{V_{obs} - V_{zi}}{V_{zi}} \times 100\% \quad (6)$$

In addition, the growth offset (τ) was defined to quantify how much the growth change that occurs due to indirect impacts on the remaining vegetation can compensate (if $\tau > 0$) or exacerbate (if $\tau < 0$) vegetation loss (i.e., V_v-V_{zi}) by land conversion (Eq. (7)):

$$\tau = \frac{V_{obs} - V_{zi}}{V_v - V_{zi}} \times 100\% \quad (7)$$

2.3.3. The determination of VI values for fully vegetated areas and fully ISA

Given that the difference in observed VI values, which is caused by different types of land-cover (e.g., cropland and forest) and vegetation (e.g., grass and trees), might confuse the urbanization impact and inherent diversities, we averaged VI values with averaged ISC for the ISC bins at an interval of 0.01. The VI-ISC relationships were fitted by the cubic regression model for all years: $y = a_0 + a_1x + a_2x^2 + a_3x^3$, where y was averaged VI and x was averaged ISC. The perfect fit of the cubic regression model (n = 100, $R^2 > 0.98$, $p < 0.001$ of EVI and GPP for all years) indicated significant correlation between vegetation growth and ISC.

We used the intercepts of regressions to determine V_v for each year, as the intercepts of regressions relied on the trend of VI change and were less affected by VI outliers (Jia et al., 2018; Zhao et al., 2016). As small vegetation patches were often fragmented and dispersive in highly urbanized environment of Shanghai, we manually selected 30 pixels associated with the fully ISA conditions for each year (510 pixels in total) by checking the high-resolution Google Earth imagery to avoid uncertainties sourced from the IS maps, and the mean VI values were calculated to determined VI_{nv}. The resultant mean EVI value (EVI_{nv}) was 0.072, and the mean GPP value (GPP_{nv}) was 92.11 $g{\cdot}m^{-2}{\cdot}year^{-1}$.

3. Results

3.1. Annual maps of impervious surfaces during 2000–2016 at 30-m spatial resolution

According to the annual maps of impervious surfaces in 2010 (Fig. 3a) and 2016 (Fig. 3b), the impervious surfaces in Shanghai were mostly distributed in the central city and inner suburbs in 2010 and expanded to the outer suburbs in 2016, especially in the Pudong, Fengxian, Jinshan, Qingpu and Chongming districts. Accuracy assessments of the annual impervious surface maps in 2010 and 2016 show high consistency between the classification maps and ground reference data for IS area (Table 2). The user accuracies of IS are 90.02% and 89.91% in 2010 and 2016, respectively, and the producer accuracies are 90.72% and 90.46%. The overall accuracies are 91.81% and 91.52%, respectively, and Kappa coefficients are 0.83 for both 2010 and 2016 IS maps.

We combined all of the annual maps of IS to illustrate the spatial-temporal patterns of IS expansion from 2000 to 2016 (Fig. 3c). The total ISA in Shanghai increased from 1587.64 km^2 in 2000 to 3097.83 km^2 in 2016, an increase of 95% (Fig. 3d). According to the interannual dynamics of newly increased ISA shown in Fig. 3c and d, we can divide the dynamics of IS expansion into three stages (namely, 2000–2004, 2004–2013 and 2013–2016). The slopes of three linear regressions were 226.9 ($R^2 = 0.975$, $p = 0.001$), 70.7 ($R^2 = 0.983$, $p < 0.001$) and 6.8 ($R^2 = 0.874$, $p = 0.04$), indicating the different growth rates of three stages. During the first stage, the ISA increased rapidly and was mainly distributed in the peri-urban areas centered around the core urban area. During the second stage, the pace of IS expansion gradually slowed, but covered more rural areas. During the third stage, the ISA expansion nearly stabilized.

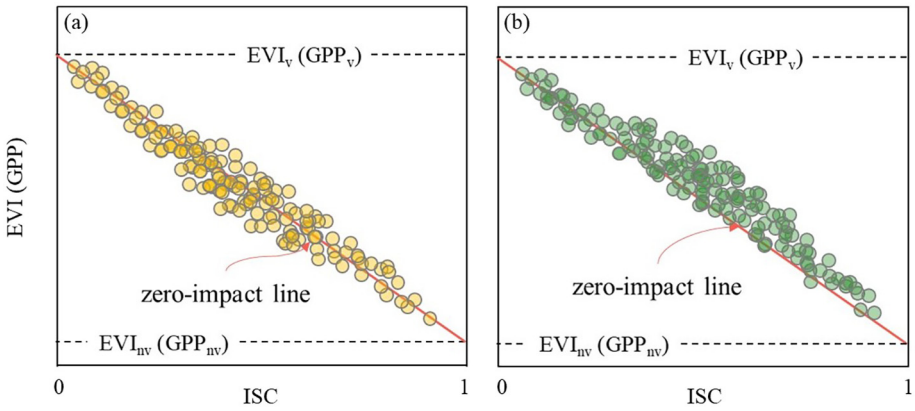

Fig. 2. The theory on the changes of EVI and GPP along the impervious surface coverage (ISC) gradient under (a) direct impact and (b) combination of both direct and indirect impact of urbanization.

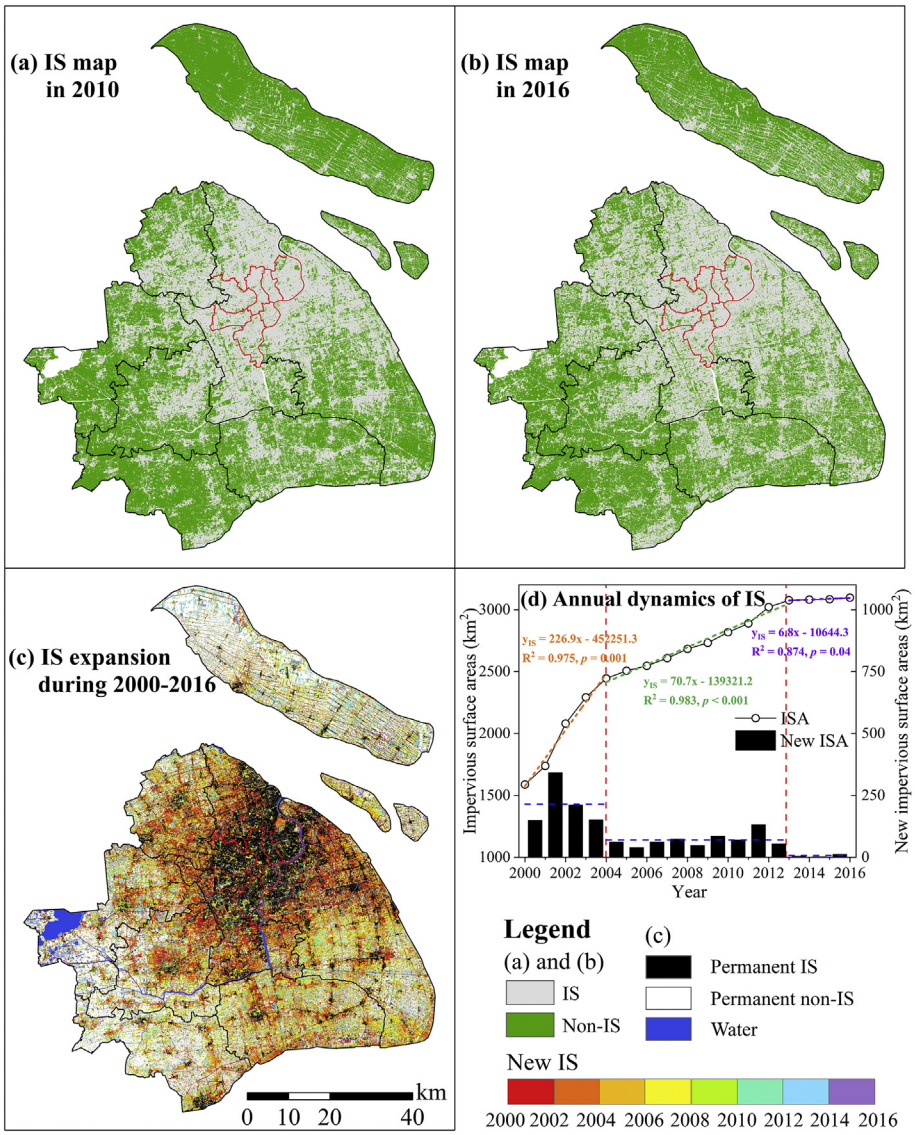

Fig. 3. Spatial distribution of impervious surface (IS) in Shanghai derived from Landsat images. IS maps in 2010 (a) and 2016 (c); expansion (c) and annual dynamics (d) of IS in Shanghai during 2000–2016.

Table 2
Accuracy assessment of impervious surface (IS) maps in 2010 and 2016, using the ground reference data selected from very high spatial resolution images in Google Earth.

Year	Land use	User accuracy/commission error (%)	Producer accuracy/omission error (%)	Overall accuracy (%)/Kappa coefficient
2010	IS	90.02/9.98	90.72/9.28	91.81/0.83
	Non-IS	93.14/6.86	92.61/7.39	
2016	IS	89.91/10.09	90.46/9.54	91.52/0.83
	Non-IS	92.75/7.25	92.33/7.67	

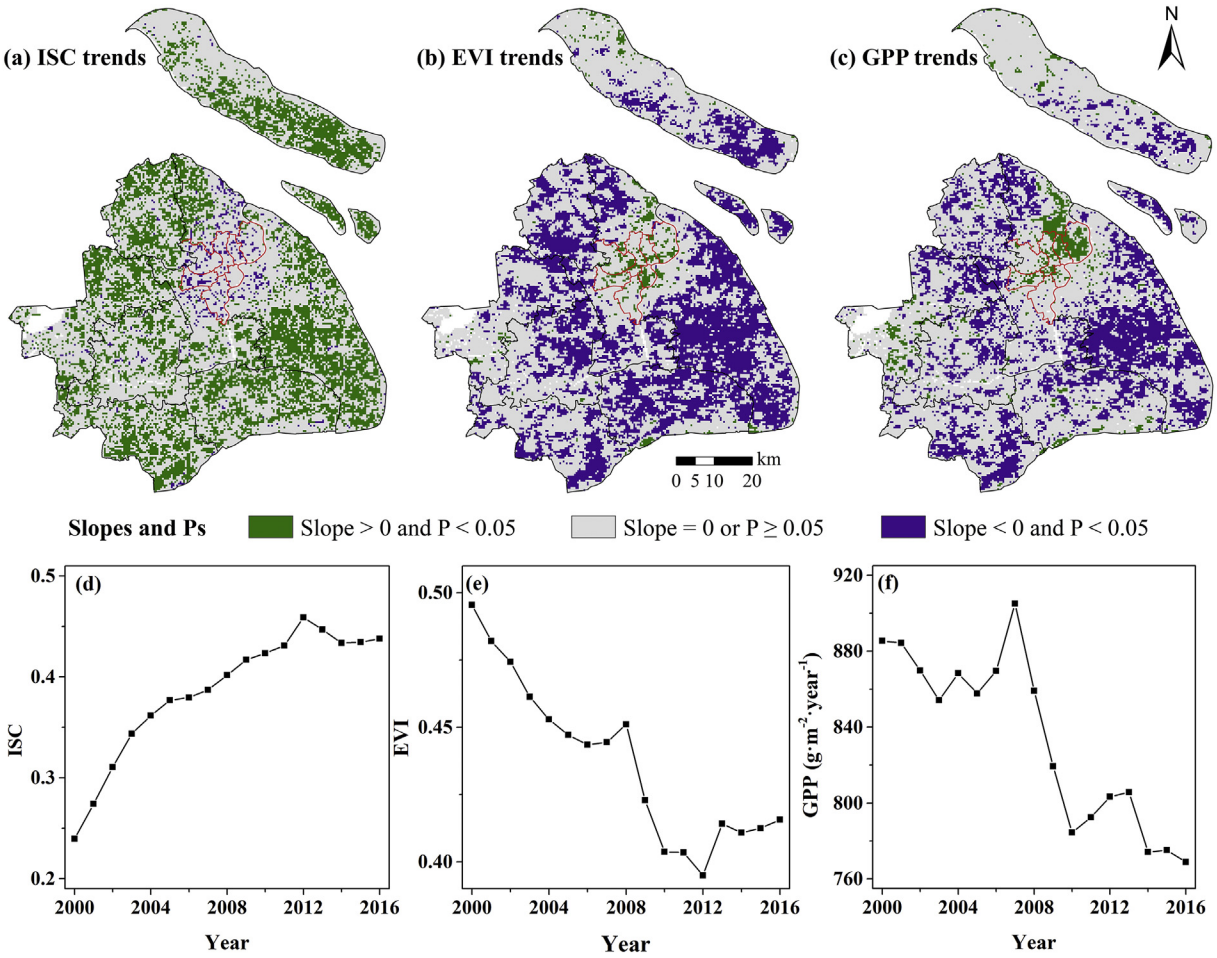

Fig. 4. The trends of (a) ISC, (b) EVI and (c) GPP at 500-m gridcells and annual dynamics of mean (e) ISC, (f) EVI and (g) GPP in Shanghai from 2000 to 2016.

3.2. Interannual variation and trends of ISC, EVI and GPP during 2000–2016 within 500-m gridcells

The analyses of ISC interannual trends within individual 500-m gridcells (a total of 28,113 gridcells) during 2000–2016 show that 37.6% gridcells had significant increasing trends, and only 2.4% gridcells in the central city had decreasing trends (Fig. 4a). As expected, the trends of EVI in most gridcells were the opposite of the trends of ISC: 38.0% gridcells showed significant decreasing trends of EVI in the peri-urban and rural areas, but only 2.8% gridcells showed increasing trends in the central city from 2000 to 2016 (Fig. 4b). Surprisingly, a fair amount (4.6%) of gridcells with significant increasing GPP trends were found in the urban core area while there were many fewer decreasing trends in other districts, 10% less than EVI (Fig. 4c). As a whole, the mean ISC showed a significant jump from 0.24 in 2000 to 0.43 in 2016 (Fig. 4d). With rapid and extensive urban expansion, the overall conditions of vegetation showed a progressive decline. EVI and GPP both fluctuated slightly with more-or-less downward trends. The mean EVI of Shanghai varied between 0.5 in 2000 and 0.42 in 2016, a decrease of 16% (Fig. 4e). The mean annual GPP of Shanghai ranged from 885 $g{\cdot}m^{-2}{\cdot}year^{-1}$ in 2000 to 769 $g{\cdot}m^{-2}{\cdot}year^{-1}$ in 2016, a decrease of 13% (Fig. 4f).

The linear regression models between EVI and ISC showed significant negative correlations (slope < 0 and $p < 0.05$) in Shanghai for the 28,113 500-m pixels (Fig. 5a and b), mostly in peri-urban areas. The linear regression models between GPP and ISC showed 28.0% significant negative correlations (slope < 0 and $p < 0.05$) of all pixels (Fig. 5c and d). Although significant negative correlations were found in mean EVI, GPP and ISC, the determination coefficients (R^2) of GPP and ISC were significantly lower than those of EVI and ISC (Fig. 5e and f), indicating that the decline in EVI could be explained well by urban expansion, whereas the change in GPP was not entirely caused by urbanization in Shanghai from 2000 to 2016.

3.3. The impacts of urbanization on EVI and GPP dynamics during 2000–2016 within 500-m gridcells

The relationships of EVI-ISC and GPP-ISC during 2000–2016 are

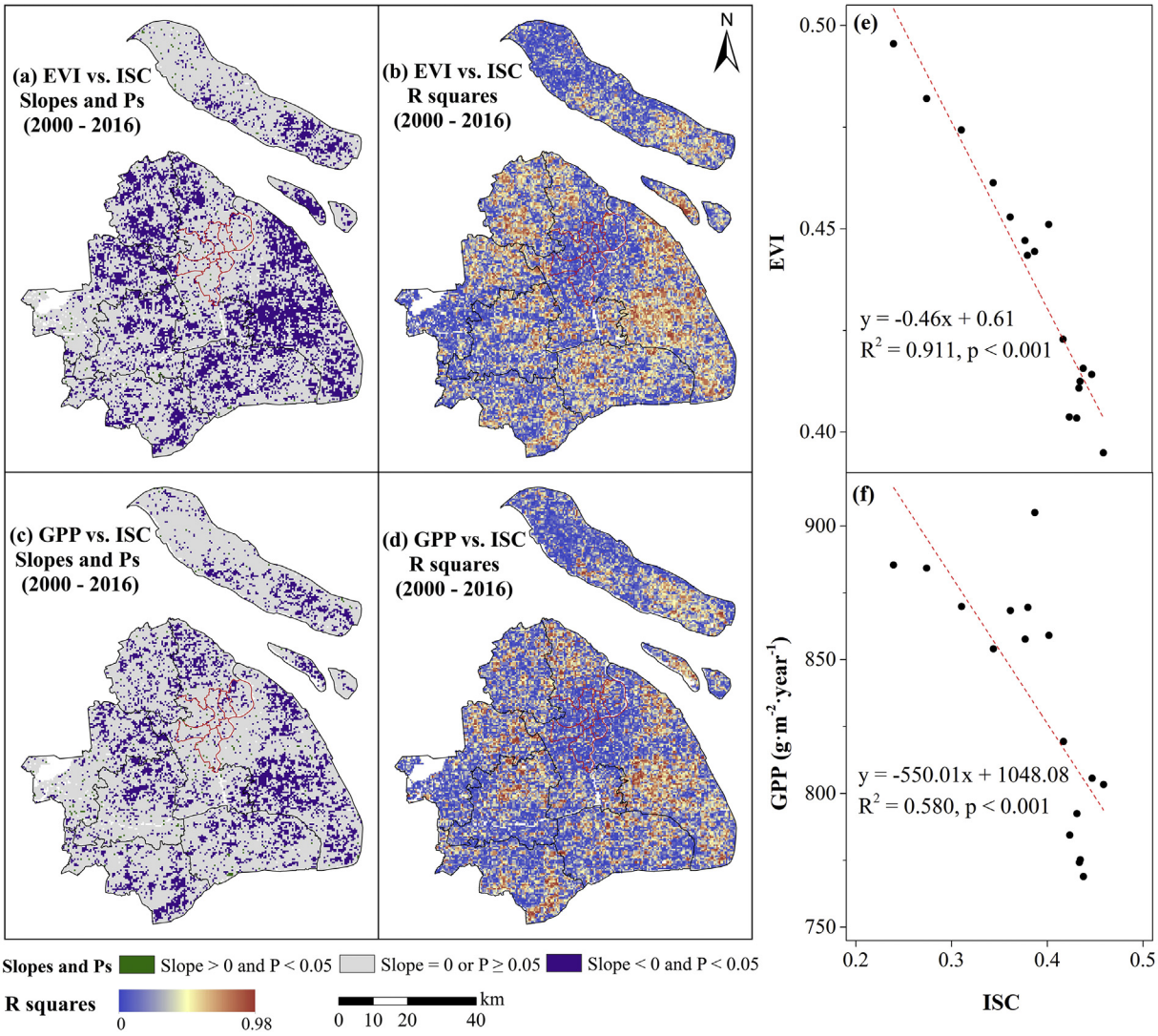

Fig. 5. The relationships between (a, b) EVI and ISC, (c, d) GPP and ISC at 500-m gridcells, and (e) mean EVI and ISC, (f) mean GPP and ISC in Shanghai from 2000 to 2016.

shown in Figs. 6 and S1. We found that the distribution of 500-m resolution pixels presented a shift from low ISC to medium-high ISC from 2000 to 2016, representing the process of urban expansion. The averaged EVI and GPP observations decreased as the ISC increased, and the cubic regressions of the EVI-ISC and GPP-ISC curves were statistically significant ($R^2 > 0.98, p < 0.001$) for all years. 92%, 88% and 94% of averaged EVI values were higher than the zero-impact lines in 2000, 2008 and 2016, respectively, while 89%, 89% and 95% for GPP, clearly suggesting the positive impact of urbanization on vegetation greenness and GPP.

The patterns of the indirect impacts of urbanization and the growth offset were captured by the illustrative examples in 2000, 2008 and 2016 (Fig. 7). The variations of the absolute change along the ISC gradient were similar for both EVI and GPP. The absolute changes of EVI and GPP observations were close to zero, with almost all the negative values distributing over the ISC of 0–0.2, suggesting that some vegetation in the low ISC areas was negatively affected by urbanization (Fig. 7a and d). The ISC value of 0.2 seems to be a threshold value where indirect impacts began to appear, indicating human management and an urban environment. The absolute changes of EVI and GPP then increased and peaked at ISC values of ~0.84 and ~0.76, respectively.

The relative indirect impact on EVI increased along the ISC gradient and reached the maximum of 57.1%, 90.3% and 107.6% at the ISC of 0.81, 0.97 and 0.98 in 2000, 2008 and 2016, while the indirect impact on GPP reached the greater maximum of 61.9%, 165.7% and 149.7% at the ISC of 0.80, 0.97 and 0.94 in 2000, 2008 and 2016 (Fig. 7b and e). Both the growth offset of EVI and GPP showed increases, being stable and falling along the ISC gradient (Fig. 7c and f). The stable state mainly occurred in medium-high ISC bins (0.3–0.8), indicating that the growth offset in suburbs was higher than in rural and highly urbanized areas. The averages of growth offset were 20.8%, 24.1% and 29.0% for EVI in 2000, 2008 and 2016, while 11.4%, 18.5% and 21.0% for GPP, which were lower than EVI. The results indicated that the positive indirect impact of urbanization on EVI became gradually stronger in 2000, 2008 and 2016, especially in the high ISC areas, but the impact on GPP in the high ISC areas was weaker in 2016 than in 2008.

4. Discussion

4.1. Spatial-temporal dynamics of impervious surface in Shanghai during 2000–2016

A number of studies have used remote sensing images and various algorithms to estimate impervious surface areas (ISA) (or urban areas) in Shanghai (Table 3) (Fan et al., 2017; Haas et al., 2015; Shi et al., 2018; Wang et al., 2017; J. Yin et al., 2011; Zhang et al., 2011; Zhao

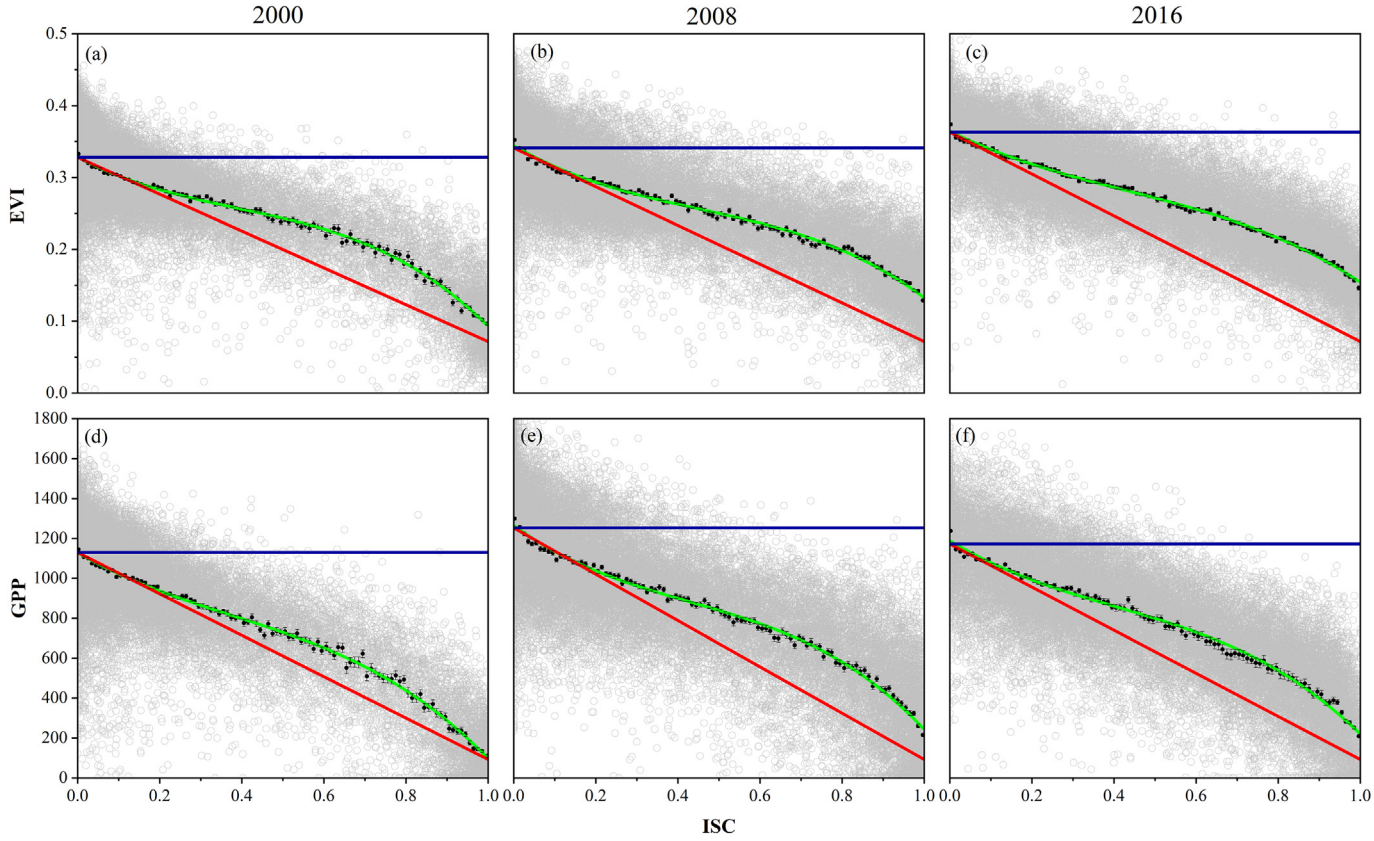

Fig. 6. Illustrative examples of the relationships between (a, b and c) EVI~ISC and (d, e and f) GPP~ISC in Shanghai in 2000, 2008 and 2016. The grey circles represent 500-m resolution pixels (n = 28,113), and black circles with error bar are the averaged EVI (GPP) with the averaged ISC of each ISC bin with an interval of 0.01 (n = 100). The green, blue and red lines are the cubic regression of the averaged EVI (GPP) ($p < 0.001$ for all regressions), background EVI and GPP V_v (i.e., the intercepts of the regressions), and zero-impact lines, respectively. (For interpretation of the references to colour in this figure legend, the reader is referred to the web version of this article.)

et al., 2006). Haas et al. (2015) reported that the amount of urban areas increased by 1130 km^2 from 2000 to 2009, and Shi et al. (2018) reported that the city added 1009.46 km^2 to urban built-up land during the decade 2000–2010. Our results showed that ISA had increased by 1144.92 km^2 from 2000 to 2009 and 1230.63 km^2 from 2000 to2010, respectively, which are slightly larger than the estimates of previous studies. The discrepancy of impervious surface maps between our studies and the previous studies can be attributed in part to (1) numbers of images used in land cover classification and (2) definition of impervious surface areas. In our study, we used all available Landsat images, which reduced the number of no-data pixels due to cloud cover and shadow. In our study we include those bare land and long-term fallow fields in the IS maps, as they were the consequences of the human-induced vegetation cover loss and would be likely converted into impervious surface as urbanization continued (Ying et al., 2017).

The annual impervious surface maps at 30-m spatial resolution and annual temporal resolution provided new insight on the process of urbanization in Shanghai over three distinct periods between 2000 and 2016. The increase of ISA in each period was largely affected by policies and socio-economic development (Z. Yin et al., 2011). After the abolition of welfare housing policy in 1998, Shanghai implemented real estate as the pillar industry of the 10th Five-Year Plan and adopted a series of measures to stimulate the development of the housing market. Driven by the policy planning and the real estate industry, urban expansion in Shanghai reached a new peak with extensive residential areas, industrial parks and various functional areas around the central city from 2000 to 2004. Over years, the in-balance between the supply and demand of land resources was increasingly prominent. In order to protect cultivated land and meet the construction requirements of major industrial projects, such as the 2010 Shanghai World Exposition and large airports, Shanghai began to strictly control the pace of new construction land and advocated the compact urban land development in 2006 (Shanghai Planning and Land Resource Administration Bureau, 2006). To some extent, our study revealed the positive effect of land planning in controlling construction land growth.

4.2. The impacts of urbanization on vegetation greenness in Shanghai

Vegetation indices (e.g., NDVI, EVI) were often used to assess the impacts of urbanization on vegetation greenness. Cui and Shi (2012) calculated mean annual NDVI of Shanghai for 1999–2001 and 2008–2010, using 10-day SPOT-4 VGT NDVI data at 1-km resolution, and found that the area with high NDVI (> 0.3) decreased from 85.8% of the total area in 1999–2001 to 76.2% in 2008–2010, whereas the area with low NDVI (0.1–0.3) increased from 12.5% of the total area to 22.6% due to urban expansion. Liu and Gong (2012) analyzed MODIS NDVI data (500-m pixel resolution) during 2000–2010 and presented a few increasing trends in the central city and extensive decreasing trends in the other districts of Shanghai. Our study reported the annual trends of EVI during 2000–2016, which offers more insights on the effect of urbanization on vegetation greenness over years. In contrast, from all of the observations from the 32 cities in China, Zhao et al. (2016) found that the positive effect of urbanization (i.e., effects other than the replacement of vegetation with IS) on vegetation greenness, including Shanghai in 2001, 2006 and 2011. Our study lends strong support to Zhao's research (Fig. S1), suggesting that urbanization could benefit the growth of urban vegetation from the perspective of canopy structure at a finer resolution and a larger temporal scale.

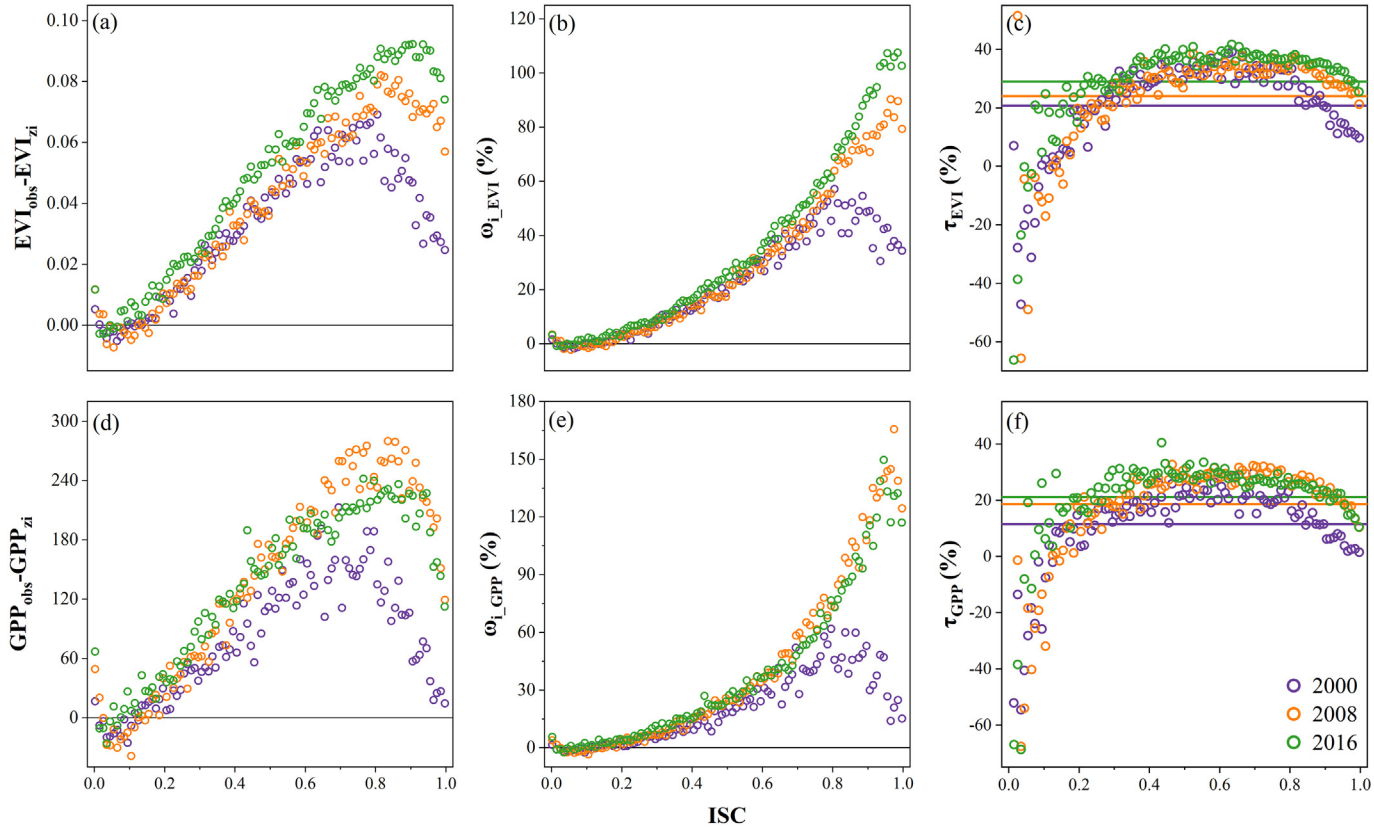

Fig. 7. Indirect impacts of urbanization on EVI and GPP along the ISC gradient in Shanghai in 2000 (violet circle), 2008 (orange circle) and 2016 (green circle): (a) the absolute EVI change (EVI_{obs} – EVI_{zi}), (b) ω_{i_EVI} (the relative indirect impact on EVI), (c) τ_{EVI} (the growth offset of EVI), (d) the absolute GPP change (GPP_{obs} – GPP_{zi}), (e) ω_{i_GPP} (the relative indirect impact on GPP), (f) τ_{GPP} (the growth offset of GPP). The mean values of the growth offset were showed with violet, orange and green lines for 2000, 2008 and 2016, respectively. (For interpretation of the references to colour in this figure legend, the reader is referred to the web version of this article.)

The increasing trend of greenness in the downtown areas from 2000 to 2016 could be explained by the Shanghai's Five-Year Plans for ecological and environmental protection, which were committed to constructing large public green spaces in the central city to increase urban green areas. As the result, many scattered and new green spaces were constructed over the last two decades (Wang et al., 2013), which clearly contributed to the increasing trend of EVI. In addition, the dominant land-use types differed clearly in Shanghai (Fig. S2), and each land use has distinct features that determines the vegetation types and the availability and allocation of growing space (Nowak et al., 1996). Species composition and density affect all structural variables (e.g., leaf area index, greenness) and urban ecosystem services (e.g., carbon sequestration and storage), because different species have distinct size profiles and traits (Graça et al., 2018; Xu et al., 2010). In Shanghai, the public green spaces in peri-urban areas, such as parks, street greenbelts and river banks, where canopy closure and community density are relatively high, would offer more favorable habitats for vegetation greenness and carbon stocks.

4.3. The impacts of urbanization on vegetation GPP in Shanghai

Considering the importance of the carbon cycle in the urban ecosystem, we used annual GPP to represent the photosynthetic uptake of carbon by vegetation and an indicator of vegetation conditions and dynamics in Shanghai from 2000 to 2016. Currently, the GPP products generated by VPM model have not been validated in urban ecosystems using eddy flux data, as few or no urban eddy flux tower sites were operated for years in the world. However, the temporal consistency between GPP_{VPM} and SIF has been reported (Cui et al., 2017; Ma et al., 2018). To assess the reliability of GPP_{VPM} data, we could use SIF data from TROPOMI mission in the near future, which has SIF data at both ungridded format and gridded format.

Cui et al. (2017) reported that Shanghai had statistically significant linear decreases in annual GPP from 2000 to 2014 and that Shanghai has experienced a large loss of total annual GPP from 7.78 in 2000 to 6.28 TgC $year^{-1}$ in 2014. Our results found the same interannual variation of annual GPP and showed that most decreasing trends

Table 3
The comparisons of urban area in Shanghai from this study with other studies and Statistical Bureau.

Year	Fan et al., 2017: urban built-up land area (km^2)	Haas et al., 2015: the ratio of urban land	J. Yin et al., 2011: urban area (km^2)	Wang et al., 2017: IS area (km^2)	Statistical Bureau: construction land (km^2)	Our study: IS area (km^2) (ISC)
2000	1625.61	0.305	1529.43	/	/	1587.64 (0.239)
2002	/	/	/	1234.40	/	2080.54 (0.310)
2007	/	/	/	2296.98	2429.08	2609.15 (0.387)
2009	/	0.470	2968.01	/	2830.00	2732.57 (0.417)
2010	2859.90	/	/	/	2891.20	2818.27 (0.423)
2013	/	/	/	2351.56	3020.00	3076.22 (0.447)

occurred in the peri-urban and rural areas at 500-m resolution; these results were closely related to the increasing trends of ISA (Fig. 3c). Comparing to EVI, the more increasing GPP trends and less decreasing trends were found in the urban core area and other districts. Probably it's because the reflection of EVI become week in dense or closed canopies with its saturation effect (Huete et al., 2002). That may suggest that annual GPP is a more valid and sensitive indicator for assessing urban vegetation condition than greenness, although the common greenness indices (e.g., NDVI and EVI) were effective enough to map the green spaces. Recent studies have also reported such negative effects of land use and cover conversion on GPP from cities in Wuhan and Denpasar (Liu et al., 2018; Nuarsa et al., 2018).

However, there is still a need to separate the effects of land use changes from other environmental changes. Using eddy flux observations and remote sensing data, Xu et al. (2017) reported that land use changes reduced the regional net ecosystem production (NEP) (NEP = GPP - respiration) of the Taihu Lake Basin (including Shanghai) from 14.3 TgC in 2000 to 12.1 TgC in 2010, whereas increasing atmospheric CO_2 concentrations and nitrogen deposition compensated for half of the total carbon loss. CO_2 eddy flux study found that the annual GPP of temperate deciduous forests was approximately 26% higher ($p < 0.05$) at the urban site of Nagoya (16.89 t C ha^{-1} $year^{-1}$) than at the rural site of Toyota (12.46 t C ha^{-1} $year^{-1}$), suggesting a possible CO_2 fertilization effect in photosynthesis due to elevated CO_2 levels in urban areas (Awal et al., 2010). Our results strongly support that the absolute enhancement of annual GPP increased along the ISC (rural-urban) gradient but declined when ISC exceeded the threshold of ~0.76 (Fig. 7d). One of the driving factors might be the spatial-distribution of atmospheric CO_2 concentration in Shanghai, as the highest near-surface atmospheric CO_2 concentration occurred in a moderately urbanized area (423.9 ± 29.3 ppm), where there are extensive areas of transportation and industrial land use types (Liu et al., 2016; Pan et al., 2016). The results from this study clearly reveal the hot-spots of the changes in annual GPP in Shanghai at 500-m spatial resolution.

We can conclude that urbanization has already altered the terrestrial carbon cycle, especially the carbon loss caused by land conversion. However, we can still maximize urbanization-induced environmental changes to promote carbon sequestration in urban ecosystems through effective protection, management and design, as urban green spaces have a range of benefits for human health and well-being under the potential pressure brought by urbanization (Douglas et al., 2017; van den Berg et al., 2015; White et al., 2019; Wood et al., 2017). Our findings could provide several valuable guidance for urban vegetation management: 1) the efforts to preserve remnant forest should be tantamount to planting young trees in a city; 2) it is recommendable to arrange green spaces close to the city center to strengthen their carbon fixing capacity; 3) the vegetation types and species selection should also be taken into consideration as they have different responses to urbanization (Escobedo et al., 2010; Shen et al., 2008; C. Zhang et al., 2014). Plant species richness is higher in cities than in surrounding rural areas due to a high rate of alien species brought into cities by humans (Wania et al., 2006; D. Zhang et al., 2016). However, a meta-analysis reported that urban planners tend to select greening plants that are highly profitable and have aesthetic ornamental properties, resulting in the trend of homogenization in urban plant communities in China (Qian et al., 2016). It can be said, humans play a key role in deciding the positive or negative impacts of urbanization on urban green spaces across a city. Given the findings in this study, the importance of positive impact of urbanization on urban vegetation should attract wider attention of local urban planners and global urban scholar communities.

5. Conclusions

In this study, we used time series Landsat and MODIS images in Shanghai during 2000–2016 to characterize the urban expansion (as measured by impervious surface area), vegetation greenness (EVI) and GPP. We quantified the negative and positive effects of urban expansion (increasing ISA) on vegetation greenness and GPP in Shanghai during 2000–2016. The interannual variation and trends of ISC, EVI and GPP showed the massive vegetation and carbon loss caused by land use conversion in peri-urban and rural areas. The urban-rural gradient analysis showed that the urban environment and human management resulted in notable enhancement, and growth offset of EVI and GPP were high in medium-high ISC areas, but low in the areas with very high ISC or very low ISC. This study has identified the hot-spots of the changes in ISC, greenness and GPP in Shanghai during 2000–2016 at 30-m and 500-m spatial resolution, which are useful for local urban planners and stakeholders to better manage urban vegetation in Shanghai, where approximately 26 million people currently live.

This study is a successful first attempt that demonstrates the potential of our research approach that uses (1) time series Landsat and MODIS images, (2) Google Earth Engine, (3) pixel- and phenology-based land cover mapping algorithms, (4) data-driven model (VPM), and (5) the conceptual framework for identifying negative and positive effect of urbanization on vegetation greenness and GPP in evaluating vegetation structure and function in the area that experienced rapid changes in rural, peri-urban and urban environment. Although the results from this study are specific to Shanghai, the methodology illustrated here could be readily applied in many other cities, to explore that if the conditions of urban vegetation are associated with different geographical environments and development patterns.

Acknowledgements

This research was supported by Natural Science Foundation of China (41601181, 41571408), National Key Research and Development Program of China (2017YFC1200100), and Open Research Fund of Guangxi Key Laboratory of Water Engineering Materials and Structures, Guangxi institute of water resources research (GXHRI-WEMS-2019-02). We thank all the reviewers for their valuable comments on the earlier versions of the manuscript.

Appendix A. Supplementary data

Supplementary data to this article can be found online at https://doi.org/10.1016/j.rse.2019.111374.

References

Akbari, H., 2002. Shade trees reduce building energy use and CO2 emissions from power plants. Environ. Pollut. 116, S119–S126.

Arnold, C.L., Gibbons, C.J., 1996. Impervious surface coverage: the emergence of a key environmental indicator. American Planning Association. J. Am. Plan. Assoc. 62, 243 Chicago.

Awal, M.A., Ohta, T., Matsumoto, K., Toba, T., Daikoku, K., Hattori, S., Hiyama, T., Park, H., 2010. Comparing the carbon sequestration capacity of temperate deciduous forests between urban and rural landscapes in central Japan. Urban For. Urban Green. 9, 261–270. https://doi.org/10.1016/j.ufug.2010.01.007.

van den Berg, M., Wendel-Vos, W., van Poppel, M., Kemper, H., van Mechelen, W., Maas, J., 2015. Health benefits of green spaces in the living environment: a systematic review of epidemiological studies. Urban For. Urban Green. 14, 806–816. https://doi.org/10.1016/j.ufug.2015.07.008.

Calfapietra, C., Penuelas, J., Niinemets, U., 2015. Urban plant physiology: adaptation-mitigation strategies under permanent stress. Trends Plant Sci. 20, 72–75. https://doi.org/10.1016/j.tplants.2014.11.001.

Chen, T., Huang, Q., Liu, M., Li, M., Qu, L., Deng, S., Chen, D., 2017. Decreasing net primary productivity in response to urbanization in Liaoning Province, China. Sustainability 9, 162. https://doi.org/10.3390/su9020162.

Cui, L., Shi, J., 2012. Urbanization and its environmental effects in Shanghai, China. Urban Clim. 2, 1–15. https://doi.org/10.1016/j.uclim.2012.10.008.

Cui, Y., Xiao, X., Zhang, Y., Dong, J., Yuanwei, Qin, Doughty, R.B., Zhang, G., Wang, J., Wu, X., Yaochen, Qin, Zhou, S., Joiner, J., Moore, B., 2017. Temporal consistency between gross primary production and solar-induced chlorophyll fluorescence in the ten most populous megacity areas over years. Sci. Rep. 7, 14963. https://doi.org/10.1038/s41598-017-13783-5.

Deng, X., Huang, J., Rozelle, S., Zhang, J., Li, Z., 2015. Impact of urbanization on cultivated land changes in China. Land Use Policy 45, 1–7. https://doi.org/10.1016/j.

landusepol.2015.01.007.
Dewan, A.M., Yamaguchi, Y., 2009. Land use and land cover change in Greater Dhaka, Bangladesh: using remote sensing to promote sustainable urbanization. Appl. Geogr. 29, 390–401. https://doi.org/10.1016/j.apgeog.2008.12.005.
Donovan, G.H., Butry, D.T., 2010. Trees in the city: valuing street trees in Portland, Oregon. Landscape & Urban Planning 94, 77–83.
Douglas, O., Lennon, M., Scott, M., 2017. Green space benefits for health and well-being: a life-course approach for urban planning, design and management. Cities 66, 53–62. https://doi.org/10.1016/j.cities.2017.03.011.
Dwyer, J.F., Mcpherson, E.G., Schroeder, H.W., Rowntree, R.A., 1992. Assessing the benefits and costs of the urban forest. Transportation Research Economics & Policy 18, 751–768.
Escobedo, F., Varela, S., Zhao, M., Wagner, J.E., Zipperer, W., 2010. Analyzing the efficacy of subtropical urban forests in offsetting carbon emissions from cities. Environ. Sci. Pol. 13, 362–372. https://doi.org/10.1016/j.envsci.2010.03.009.
Fan, P., Xu, L., Yue, W., Chen, J., 2017. Accessibility of public urban green space in an urban periphery: the case of Shanghai. Landsc. Urban Plan. 165, 177–192. https://doi.org/10.1016/j.landurbplan.2016.11.007.
Foga, S., Scaramuzza, P.L., Guo, S., Zhu, Z., Dilley, R.D., Beckmann, T., Schmidt, G.L., Dwyer, J.L., Hughes, M.J., Laue, B., 2017. Cloud detection algorithm comparison and validation for operational Landsat data products. Remote Sens. Environ. 194, 379–390. https://doi.org/10.1016/j.rse.2017.03.026.
Gao, B., 1996. NDWI—a normalized difference water index for remote sensing of vegetation liquid water from space. Remote Sens. Environ. 58, 257–266.
Graça, M., Alves, P., Gonçalves, J., Nowak, D.J., Hoehn, R., Farinha-Marques, P., Cunha, M., 2018. Assessing how green space types affect ecosystem services delivery in Porto, Portugal. Landsc. Urban Plan. 170, 195–208. https://doi.org/10.1016/j.landurbplan.2017.10.007.
Guan, X., Shen, H., Li, X., Gan, W., Zhang, L., 2019. A long-term and comprehensive assessment of the urbanization-induced impacts on vegetation net primary productivity. Sci. Total Environ. 669, 342–352. https://doi.org/10.1016/j.scitotenv.2019.02.361.
Haas, J., Furberg, D., Ban, Y., 2015. Satellite monitoring of urbanization and environmental impacts—a comparison of Stockholm and Shanghai. Int. J. Appl. Earth Obs. Geoinf. 38, 138–149. https://doi.org/10.1016/j.jag.2014.12.008.
Hardin, P.J., Jensen, R.R., 2007. The effect of urban leaf area on summertime urban surface kinetic temperatures: a Terre Haute case study. Urban For. Urban Green. 6, 63–72. https://doi.org/10.1016/j.ufug.2007.01.005.
Huete, A.R., Liu, H.Q., Batchily, K., van Leeuwen, W., 1997. A comparison of vegetation indices over a global set of TM images for EOS-MODIS. Remote Sens. Environ. 59, 440–451. https://doi.org/10.1016/S0034-4257(96)00112-5.
Huete, A., Didan, K., Miura, T., Rodriguez, E.P., Gao, X., Ferreira, L.G., 2002. Overview of the radiometric and biophysical performance of the MODIS vegetation indices. Remote Sens. Environ. 83, 195–213. https://doi.org/10.1016/S0034-4257(02)00096-2.
Imhoff, M.L., Bounoua, L., DeFries, R., Lawrence, W.T., Stutzer, D., Tucker, C.J., Ricketts, T., 2004. The consequences of urban land transformation on net primary productivity in the United States. Remote Sens. Environ. 89, 434–443. https://doi.org/10.1016/j.rse.2003.10.015.
Jia, W., Zhao, S., Liu, S., 2018. Vegetation growth enhancement in urban environments of the Conterminous United States. Glob. Chang. Biol. 24, 4084–4094. https://doi.org/10.1111/gcb.14317.
Jr, C.L.A., Gibbons, C.J., 1996. Impervious surface coverage: the emergence of a key environmental indicator. J. Am. Plan. Assoc. 62, 243–258. https://doi.org/10.1080/01944369608975688.
Kotarba, A.Z., Aleksandrowicz, S., 2016. Impervious surface detection with nighttime photography from the International Space Station. Remote Sens. Environ. 176, 295–307. https://doi.org/10.1016/j.rse.2016.02.009.
Li, Y., Zhao, S., Zhao, K., Xie, P., Fang, J., 2006. Land-cover changes in an urban lake watershed in a mega-city, Central China. Environ. Monit. Assess. 115, 349–359. https://doi.org/10.1007/s10661-006-6559-z.
Li, J., Wang, Z., Lai, C., Wu, X., Zeng, Z., Chen, X., Lian, Y., 2018. Response of net primary production to land use and land cover change in mainland China since the late 1980s. Sci. Total Environ. 639, 237–247. https://doi.org/10.1016/j.scitotenv.2018.05.155.
Liu, S., Gong, P., 2012. Change of surface cover greenness in China between 2000 and 2010. Chin. Sci. Bull. 57, 2835–2845. https://doi.org/10.1007/s11434-012-5267-z.
Liu, Y., Wang, Y., Peng, J., Du, Y., Liu, X., Li, S., Zhang, D., 2015. Correlations between urbanization and vegetation degradation across the world's metropolises using DMSP/OLS nighttime light data. Remote Sens. 7, 2067–2088. https://doi.org/10.3390/rs70202067.
Liu, M., Zhu, X., Pan, C., Chen, L., Zhang, H., Jia, W., Xiang, W., 2016. Spatial variation of near-surface CO2 concentration during spring in Shanghai. Atmospheric Pollution Research 7, 31–39. https://doi.org/10.1016/j.apr.2015.07.002.
Liu, S., Du, W., Su, H., Wang, S., Guan, Q., 2018. Quantifying impacts of land-use/cover change on urban vegetation gross primary production: a case study of Wuhan, China. Sustainability 10, 714. https://doi.org/10.3390/su10030714.
Lohr, V.I., Pearsonmims, C.H., Tarnai, J., Dillman, D.A., 2004. How urban residents rate and rank the benefits and problems associated with trees in cities. J. Arboric. 30, 28–36.
Lohse, K.A., Hope, D., Sponseller, R., Allen, J.O., Grimm, N.B., 2008. Atmospheric deposition of carbon and nutrients across an arid metropolitan area. Sci. Total Environ. 402, 95–105. https://doi.org/10.1016/j.scitotenv.2008.04.044.
Lovett, G.M., Traynor, M.M., Pouyat, R.V., Carreiro, M.M., Zhu, W.-X., Baxter, J.W., 2000. Atmospheric deposition to oak forests along an urban − rural gradient. Environmental Science & Technology 34, 4294–4300. https://doi.org/10.1021/es001077q.
Luedeling, E., Buerkert, A., 2008. Typology of oases in northern Oman based on Landsat and SRTM imagery and geological survey data. Remote Sens. Environ. 112, 1181–1195.
Ma, J., Xiao, X., Zhang, Y., Doughty, R., Chen, B., Zhao, B., 2018. Spatial-temporal consistency between gross primary productivity and solar-induced chlorophyll fluorescence of vegetation in China during 2007–2014. Sci. Total Environ. 639, 1241–1253. https://doi.org/10.1016/j.scitotenv.2018.05.245.
McDonnell, M.J., Pickett, S.T.A., Pouyat, R.V., 1993. The application of the ecological gradient paradigm to the study of urban effects. In: Humans as Components of Ecosystems. Springer, New York, NY, pp. 175–189. https://doi.org/10.1007/978-1-4612-0905-8_15.
Mcpherson, E., 1998. Structure and sustainability of Sacramento's urban forest. J. Arboric. 24.
Mcpherson, E.G., Simpson, J.R., 2002. A comparison of municipal forest benefits and costs in Modesto and Santa Monica, California, USA. Urban For. Urban Green. 1, 61–74.
Milesi, C., Elvidge, C.D., Nemani, R.R., Running, S.W., 2003. Assessing the impact of urban land development on net primary productivity in the southeastern United States. Remote Sens. Environ. 86, 401–410. https://doi.org/10.1016/S0034-4257(03)00081-6.
Nowak, D.J., Crane, D.E., Dwyer, J.F., 2002. Compensatory value of urban trees in the United States. J. Arboric. 28, 194–199.
Nowak, D.J., Crane, D.E., Stevens, J.C., 2006. Air pollution removal by urban trees and shrubs in the United States. Urban For. Urban Green. 4, 115–123.
Nowak, D.J., Rowntree, R.A., McPherson, E.G., Sisinni, S.M., Kerkmann, E.R., Stevens, J.C., 1996. Measuring and analyzing urban tree cover. Landsc. Urban Plan. 36, 49–57. https://doi.org/10.1016/S0169-2046(96)00324-6.
Nuarsa, I.W., As-syakur, A.R., Gunadi, I.G.A., Sukewijaya, I.M., 2018. Changes in Gross Primary Production (GPP) over the past two decades due to land use conversion in a tourism city. ISPRS Int. J. Geo Inf. 7, 57. https://doi.org/10.3390/ijgi7020057.
Pan, C., Zhu, Xiyang, Wei, N., Zhu, Xudong, She, Q., Jia, W., Liu, M., Xiang, W., 2016. Spatial variability of daytime CO2 concentration with landscape structure across urbanization gradients, Shanghai, China. Clim. Res. 69, 107–116. https://doi.org/10.3354/cr01394.
Peng, J., Shen, H., Wu, W., Liu, Y., Wang, Y., 2016. Net primary productivity (NPP) dynamics and associated urbanization driving forces in metropolitan areas: a case study in Beijing City, China. Landsc. Ecol. 31, 1077–1092. https://doi.org/10.1007/s10980-015-0319-9.
Qian, S., Qi, M., Huang, L., Zhao, L., Lin, D., Yang, Y., 2016. Biotic homogenization of China's urban greening: a meta-analysis on woody species. Urban For. Urban Green. 18, 25–33. https://doi.org/10.1016/j.ufug.2016.05.002.
Qin, Y.W., Xiao, X.M., Dong, J.W., Chen, B.Q., Liu, F., Zhang, G.L., Zhang, Y., Wang, J., Wu, X.C., 2017. Quantifying annual changes in built-up area in complex urban-rural landscapes from analyses of PALSAR and Landsat images. ISPRS J. Photogramm. Remote Sens. 124, 89–105. https://doi.org/10.1016/j.isprsjprs.2016.12.011.
Ridd, M.K., 1995. Exploring a V-I-S (vegetation-impervious surface-soil) model for urban ecosystem analysis through remote sensing: comparative anatomy for cities†. Int. J. Remote Sens. 16, 2165–2185. https://doi.org/10.1080/01431169508954549.
Roy, S., Byrne, J., Pickering, C., 2012. A systematic quantitative review of urban tree benefits, costs, and assessment methods across cities in different climatic zones. Urban For. Urban Green. 11, 351–363. https://doi.org/10.1016/j.ufug.2012.06.006.
Salvati, L., Sabbi, A., 2011. Exploring long-term land cover changes in an urban region of southern Europe. Int. J. Sustain. Dev. World Ecol. 18, 273–282. https://doi.org/10.1080/13504509.2011.560453.
Shanghai Planning and Land Resource Administration Bureau, 2006. Land use planning in Shanghai (2006–2020) [WWW document]. URL. http://www.shgtj.gov.cn/tdgl/200812/t20081223_152679.html, Accessed date: 17 November 2018.
Shanghai Statistical Bureau, 2017. Shanghai statistical yearbook in 2017 [WWW document]. http://www.stats-sh.gov.cn/html/sjfb/201801/1001529.html, Accessed date: 14 July 2018.
Shen, W., Wu, J., Grimm, N.B., Hope, D., 2008. Effects of urbanization-induced environmental changes on ecosystem functioning in the Phoenix metropolitan region, USA. Ecosystems 11, 138–155. https://doi.org/10.1007/s10021-007-9085-0.
Shi, G., Jiang, N., Yao, L., Shi, G., Jiang, N., Yao, L., 2018. Land use and cover change during the rapid economic growth period from 1990 to 2010: a case study of Shanghai. Sustainability 10, 426. https://doi.org/10.3390/su10020426.
Tucker, C.J., 1979. Red and photographic infrared linear combinations for monitoring vegetation. Remote Sens. Environ. 8, 127–150. https://doi.org/10.1016/0034-4257(79)90013-0.
United Nations, 2017. World Population Prospects: The 2017 Revision. United Nations Department of Economic and Social Affairs, Population Division, New York.
USGS, 2015. Important information: upcoming landsat data processing changes [WWW document]. https://landsat.usgs.gov/landsat-update-volume-9-issue-1-2015, Accessed date: 14 July 2018.
Vallet, J., Daniel, H., Beaujouan, V., Rozé, F., Pavoine, S., 2010. Using biological traits to assess how urbanization filters plant species of small woodlands. Appl. Veg. Sci. 13, 412–424. https://doi.org/10.1111/j.1654-109X.2010.01087.x.
Vermote, E., 2015. MOD09A1 MODIS/Terra Surface Reflectance 8-Day L3 Global 500m SIN Grid V006. https://doi.org/10.5067/MODIS/MOD09A1.006.
Wang, Z., Cui, X., Yin, S., Shen, G., Han, Y., Liu, C., 2013. Characteristics of carbon storage in Shanghai's urban forest. Chin. Sci. Bull. 58, 1130–1138. https://doi.org/10.1007/s11434-012-5443-1.
Wang, H., Zhang, Y., Tsou, J., Li, Y., Wang, H., Zhang, Y., Tsou, J.Y., Li, Y., 2017. Surface urban heat island analysis of Shanghai (China) based on the change of land use and land cover. Sustainability 9, 1538. https://doi.org/10.3390/su9091538.
Wania, A., Kühn, I., Klotz, S., 2006. Plant richness patterns in agricultural and urban landscapes in Central Germany—spatial gradients of species richness. Landsc. Urban

Plan. 75, 97–110. https://doi.org/10.1016/j.landurbplan.2004.12.006.
Weng, Q., 2012. Remote sensing of impervious surfaces in the urban areas: requirements, methods, and trends. Remote Sensing of Environment. Remote Sensing of Urban Environments 117, 34–49. https://doi.org/10.1016/j.rse.2011.02.030.
Weng, Q., Hu, X., Lu, D., 2008. Extracting impervious surfaces from medium spatial resolution multispectral and hyperspectral imagery: a comparison. Int. J. Remote Sens. 29, 3209–3232. https://doi.org/10.1080/01431160701469024.
White, M.P., Alcock, I., Grellier, J., Wheeler, B.W., Hartig, T., Warber, S.L., Bone, A., Depledge, M.H., Fleming, L.E., 2019. Spending at least 120 minutes a week in nature is associated with good health and wellbeing. Sci. Rep. 9, 7730. https://doi.org/10.1038/s41598-019-44097-3.
Wood, L., Hooper, P., Foster, S., Bull, F., 2017. Public green spaces and positive mental health – investigating the relationship between access, quantity and types of parks and mental wellbeing. Health & Place 48, 63–71. https://doi.org/10.1016/j.healthplace.2017.09.002.
Wu, C., Murray, A.T., 2003. Estimating impervious surface distribution by spectral mixture analysis. Remote Sens. Environ. 84, 493–505. https://doi.org/10.1016/S0034-4257(02)00136-0.
Xiao, X., Boles, S., Frolking, S., Salas, W., Moore, B., Li, C., Longhua, H., Zhao, R., 2002a. Landscape-scale characterization of cropland in China using Vegetation and Landsat TM images. International Journal of Remote Sensing - Int J Remote Sens 23, 3579–3594.
Xiao, X., Boles, S., Frolking, S., Salas, W., Moore, B., Li, C., Longhua, H., Zhao, R., 2002b. Observation of flooding and rice transplanting of paddy rice fields at the site to landscape scales in China using VEGETATION sensor data. International Journal of Remote Sensing - Int J Remote Sens 23, 3009–3022.
Xu, H., 2006. Modification of normalized difference water index (NDWI) to enhance open water features in remotely sensed imagery. Int. J. Remote Sens. 27, 3025–3033. https://doi.org/10.1080/01431160600589179.
Xu, C., Liu, M., An, S., Chen, J.M., Yan, P., 2007. Assessing the impact of urbanization on regional net primary productivity in Jiangyin County, China. Journal of Environmental Management, Carbon Sequestration in China's Forest Ecosystems 85, 597–606. https://doi.org/10.1016/j.jenvman.2006.08.015.
Xu, F., Liu, W., Ren, W., Zhong, Q., Zhang, G., Wang, K., 2010. Effects of community structure on carbon fixation of urban forests in Shanghai, China (in Chinese). Shengtaixue Zazhi 29, 439–447.
Xu, X., Yang, G., Tan, Y., Tang, X., Jiang, H., Sun, X., Zhuang, Q., Li, H., 2017. Impacts of land use changes on net ecosystem production in the Taihu Lake Basin of China from 1985 to 2010. Journal of Geophysical Research: Biogeosciences 122, 690–707. https://doi.org/10.1002/2016JG003444.
Yao, R., Cao, J., Wang, L., Zhang, W., Wu, X., 2019. Urbanization effects on vegetation cover in major African cities during 2001–2017. Int. J. Appl. Earth Obs. Geoinf. 75, 44–53. https://doi.org/10.1016/j.jag.2018.10.011.
Yin, Z., Yin, J., Xu, S., Liao, B., 2011a. Shanghai's urban spatio-temporal evolution and its driving forces of during the transitional period (1979–2009) (in Chinese). China Soft Science 101–109.
Yin, J., Yin, Z., Zhong, H., Xu, S., Hu, X., Wang, J., Wu, J., 2011b. Monitoring urban expansion and land use/land cover changes of Shanghai metropolitan area during the transitional economy (1979–2009) in China. Environmental Monitoring and Assessment; Dordrecht 177, 609–621. https://doi.org/10.1007/s10661-010-1660-8.
Ying, Q., Hansen, M.C., Potapov, P.V., Tyukavina, A., Wang, L., Stehman, S.V., Moore, R., Hancher, M., 2017. Global bare ground gain from 2000 to 2012 using Landsat imagery. Remote Sens. Environ. 194, 161–176. https://doi.org/10.1016/j.rse.2017.03.022.
Zhang, H., Zhou, L.-G., Chen, M.-N., Ma, W.-C., Zhang, H., Zhou, L.-G., Chen, M.-N., Ma, W.-C., 2011. Land use dynamics of the fast-growing Shanghai Metropolis, China (1979–2008) and its implications for land use and urban planning policy. Sensors 11, 1794–1809. https://doi.org/10.3390/s110201794.
Zhang, C., Tian, H., Pan, S., Lockaby, G., Chappelka, A., 2014a. Multi-factor controls on terrestrial carbon dynamics in urbanized areas. Biogeosciences 11, 7107–7124. https://doi.org/10.5194/bg-11-7107-2014.
Zhang, Y., Zhang, H., Lin, H., 2014b. Improving the impervious surface estimation with combined use of optical and SAR remote sensing images. Remote Sens. Environ. 141, 155–167. https://doi.org/10.1016/j.rse.2013.10.028.
Zhang, Y., Xiao, X.M., Zhou, S., Ciais, P., McCarthy, H., Luo, Y.Q., 2016a. Canopy and physiological controls of GPP during drought and heat wave. Geophys. Res. Lett. 43, 3325–3333. https://doi.org/10.1002/2016gl068501.
Zhang, D., Zheng, H., He, X., Ren, Z., Zhai, C., Yu, X., Mao, Z., Wang, P., 2016b. Effects of forest type and urbanization on species composition and diversity of urban forest in Changchun, Northeast China. Urban Ecosyst. 19, 455–473. https://doi.org/10.1007/s11252-015-0473-5.
Zhang, L., Weng, Q., Shao, Z., 2017a. An evaluation of monthly impervious surface dynamics by fusing Landsat and MODIS time series in the Pearl River Delta, China, from 2000 to 2015. Remote Sens. Environ. 201, 99–114. https://doi.org/10.1016/j.rse.2017.08.036.
Zhang, Y., Xiao, X.M., Wu, X.C., Zhou, S., Zhang, G.L., Qin, Y.W., Dong, J.W., 2017b. Data descriptor: a global moderate resolution dataset of gross primary production of vegetation for 2000–2016. Scientific Data 4. https://doi.org/10.1038/sdata.2017.165.
Zhao, S., Da, L., Tang, Z., Fang, H., Song, K., Fang, J., 2006. Ecological consequences of rapid urban expansion: Shanghai, China. Front. Ecol. Environ. 4, 341–346. https://doi.org/10.1890/1540-9295(2006)004[0341:ECORUE]2.0.CO;2.
Zhao, S.Q., Liu, S.G., Zhou, D.C., 2016. Prevalent vegetation growth enhancement in urban environment. Proc. Natl. Acad. Sci. U. S. A. 113, 6313–6318. https://doi.org/10.1073/pnas.1602312113.
Zhou, Y., Xing, B., Ju, W., 2015. Assessing the impact of urban sprawl on net primary productivity of terrestrial ecosystems using a process-based model—a case study in Nanjing, China. IEEE Journal of Selected Topics in Applied Earth Observations and Remote Sensing 8, 2318–2331. https://doi.org/10.1109/JSTARS.2015.2440274.
Zhu, Z., Woodcock, C.E., 2012. Object-based cloud and cloud shadow detection in Landsat imagery. Remote Sens. Environ. 118, 83–94. https://doi.org/10.1016/j.rse.2011.10.028.
Zhu, Z., Wang, S., Woodcock, C.E., 2015. Improvement and expansion of the Fmask algorithm: cloud, cloud shadow, and snow detection for Landsats 4–7, 8, and Sentinel 2 images. Remote Sens. Environ. 159, 269–277. https://doi.org/10.1016/j.rse.2014.12.014.
Zhu, Z., Fu, Y., Woodcock, C.E., Olofsson, P., Vogelmann, J.E., Holden, C., Wang, M., Dai, S., Yu, Y., 2016. Including land cover change in analysis of greenness trends using all available Landsat 5, 7, and 8 images: a case study from Guangzhou, China (2000–2014). Remote Sensing of Environment, Landsat 8 Science Results 185, 243–257. https://doi.org/10.1016/j.rse.2016.03.036.
Zou, Z.H., Dong, J.W., Menarguez, M.A., Xiao, X.M., Qin, Y.W., Doughty, R.B., Hooker, K.V., Hambright, K.D., 2017. Continued decrease of open surface water body area in Oklahoma during 1984-2015. Sci. Total Environ. 595, 451–460. https://doi.org/10.1016/j.scitotenv.2017.03.259.
Zou, Z., Xiao, X., Dong, J., Qin, Y., Doughty, R.B., Menarguez, M.A., Zhang, G., Wang, J., 2018. Divergent trends of open-surface water body area in the contiguous United States from 1984 to 2016. Proc. Natl. Acad. Sci. U. S. A. 115, 3810–3815. https://doi.org/10.1073/pnas.1719275115.